11th World Congress on Computational Mechanics (WCCM XI)
5th European Conference on Computational Mechanics (ECCM V)
6th European Conference on Computational Fluid Dynamics (ECFD VI)
E. Oñate, J. Oliver and A. Huerta (Eds)

UNSTRUCTURED 3D NUMERICAL MODELING OF THE MELTING OF A PCM CONTAINED IN A SPHERICAL CAPSULE

Pedro A. Galione[1] [3], Oriol Lehmkuhl[1] [2], Joaquim Rigola[1], Carles D. Pérez-Segarra[1], Assensi Oliva[1]

[1]Heat and Mass Transfer Technological Center (CTTC),Universitat Politècnica de Catalunya - BarcelonaTech, ETSEIAT, Colom 11, 08222, Terrassa (Barcelona), Spain.
[2] Termo Fluids S.L., Av. Jacquard 97 1-E, 08222, Terrassa (Barcelona), Spain.
[3] Instituto de Ingeniería Mecánica y Producción Industrial (IIMPI), Universidad de la República (UdelaR), Uruguay.

Key words: Multiphysics Problems, Computing Methods, Melting, PCM

Abstract.

1 INTRODUCTION

Fixed-grid enthalpy models have been used extensively for solid-liquid phase-change computational fluid dynamics (CFD) simulations. Generally, implicit time schemes are used by most authors [1, 2].

Tan et al. [2] presented an experimental and numerical study of the melting of a phase change material (PCM) contained in a spherical capsule; where a two-dimensional (2D) model was used for the numerical simulations, assuming axisymmetry with respect to the vertical axis.

This work is a continuation of an earlier work [3], which dealt with fixed-grid solid-liquid phase-change modeling using explicit time schemes, specially suited for its combination with turbulence models for simulation of the fluid motion. Here, the numerical model is applied for both 2D and 3D simulations of the experiment of Tan et al., using unstructured meshes. The 3D treatment allows to reproduce 3D flow patterns that are not simulated with the 2D models.

Some modifications to the numerical treatment presented in [3] have been necessary, in order to avoid numerical divergence in cases where dense meshes were used. These changes are related to the treatment of the momentum equation in the solid-liquid interface.

A formulation where both liquid and solid phases are assumed to have the same thermophysical properties, as well as another which accounts for their variation with phase and temperature (i.e. expansion in the melting, variation of conductivity, etc.), are numerically solved and their results compared.

Results showing the development of the interface, as well as the evolution of the temperature at some selected positions, are presented and compared against the experimental results obtained from [2].

2 MATHEMATICAL MODELING AND NUMERICAL IMPLEMENTATION

2.1 Mathematical modeling

Enthalpy formulation for the energy equation, porous medium-like formulation for the momentum equations, as in [1, 3].

The equations presented in [3] for modelling solid-liquid phase change CFD are here used and extended to variable physical properties. Specifically, the density is allowed to vary between solid and liquid phases and within the liquid phase. This introduces an important modification to the model, since the traditional incompressibility condition ($\nabla \cdot \vec{u} = 0$) is not valid anymore.

Resulting governing equations (mass, momentum and energy balances):

$$\frac{\partial \rho_m}{\partial t} + \nabla \cdot (\rho_l \vec{u}) = 0 \tag{1}$$

$$\frac{\partial \rho_l \vec{u}}{\partial t} + \nabla \cdot \left(\rho_l \vec{u} \frac{\vec{u}^*}{\epsilon} \right) = -\nabla p + \nabla \cdot (\mu_l \nabla \vec{u}) - \rho_l \epsilon \vec{g} - S\vec{u} \tag{2}$$

$$\frac{\partial \rho_m h_m}{\partial t} + \nabla \cdot (\rho_l h_l \vec{u}) = \nabla \cdot (\lambda_m \nabla T) \tag{3}$$

where:

$$\rho_m = \epsilon \rho_l + (1 - \epsilon) \rho_s$$
$$\rho_m h_m = \epsilon \rho_l h_l + (1 - \epsilon) \rho_s h_s$$

Where sub-indexes l and s indicate properties of the liquid and solid phases, respectivley; while m indicates a property of the mixture of solid and liquid phases. ϵ is the volumetric liquid fraction, which can take values between 0 (solid) and 1 (liquid). Velocity $\vec{u}$ corresponds to the seepage or Darcy velocity [4]. Enthalpy h include both liquid and sensible components.

Equation (2) corresponds to the momentum equation for porous media [5], where momentum source term coefficient S has been simplified, only accounting for the Darcian part of the drag force induced by the presence of the solid phase, as in [6].

2.2 Numerical issues

The formulation presented above has been implemented into the CFD computer package TermoFluids [7], which is designed to work with unstructured meshes. A collocated discretization and explicit time schemes have been used, with the time step dynamically

adapted by estimating upper bounds for the eigenvalues of convective and diffusive operators [8]. The code is parallelized and can be run both on single computers as well as in computing clusters.

Regarding the numerical treatment of the liquid-solid interface cells, some modifications have been performed with respect to that presented in [3]. In the course of running 3D cases with dense meshes, divergence occurred in several occations. A close examination of the problematic cells (where divergence started) allowed to observe that they were liquid cells forming "holes" in the solid structure; i.e. they where liquid cells which where in contact with one solid cell and with another liquid cell which was also in contact with another solid cell.

The solution to the problem was to "alleviate" the internal solid boundary condition mentioned in [3] for the pressure. This boundary condition, if applied to internal solid boundaries (in faces shared by liquid and solid cells) in the same way as for the domain solid boundaries, enforces cell velocities to be parallel to the solid faces. This results in a velocity field of the liquid —near the solid phase— that changes direction according to the shape of the solid cells, which are highly irregular, specially in the case of a 3D unstructured spherical capsule. We believe that this high fluctuation of the velocity field (from cell to cell) may produce an ill-conditioning of the Poisson-like system of pressure equations.

Instead of directly imposing the solid boundary condition to the internal solid faces, a different approach has been adopted. Solid cells in contact with liquid-containing cells are introduced into the system of pressure equations; i.e. pressure is calculated in such cells as in the liquid-containing sub-system of cells/equations. Mass flow is allowed to be different from zero in solid/liquid faces, being determined by the solution of the Poisson-like system enforcing mass balance, allowing it to "trespass" solid cells. However, centered cell velocities in these special solid cells are explicitly set to zero.

This approach solves the above-mentioned divergence problems and results in a much "smoother" and more realistic velocity field in the proximity of solid cells.

Numerical implementation of the mass balance, due to density variations, is modified in the following manner:

$$\frac{\rho_m^{n+1} - \rho_m^n}{\Delta t} = -\nabla \cdot (\rho_l^{n+1} \vec{u}^{n+1}) \tag{4}$$

Resulting in a modified version of the Poisson-like equations from those presented in [3]:

$$\Delta t \nabla \cdot \left(\frac{\nabla p^{n+1}}{1 + \Delta t S} \right) = \nabla \cdot \left(\frac{u^p}{1 + \Delta t S} \right) + \frac{\rho_m^{n+1} - \rho_m^n}{\Delta t} \tag{5}$$

where, using Adams-Bashforth 2$^{\text{nd}}$ order time integration scheme:

$$\rho_l u^p = \rho_l \vec{u}^n + \Delta t \left[\frac{3}{2} R^n(\vec{u}) - \frac{1}{2} R^{n-1}(\vec{u}) \right] \tag{6}$$

is a pseudo-predictor velocity, and thus:

$$\rho_l u^{n+1} = \left(\frac{\rho_l u^p - \Delta t \nabla p^{n+1}}{1 + \Delta t S} \right) \tag{7}$$

from where the new velocity field (u^{n+1}) is calculated. R is the sum of convective, diffusive and buoyancy source terms.

3 CASES DEFINITION

2D and 3D meshes have been used for studying the melting of n-Octadecane in a spherical capsule. Table 1 shows the list of meshes used, assigning a code for each one.

Table 1: Meshes used

Code	Cells	Cells for opening	Prismatic layers	Smallest[a]	Biggest[a]
2D-NO-7.7E3	7669	-	-	5.75E-5	4.8E-3
2D-NO-31E3	30670	-	-	1.3E-5	1.3E-3
2D-WO-5.3E3	5340	400	-	3.7E-5	9.2E-4
2D-WO-9.3E3	9257	400	-	2.63E-5	1.3E-3
2D-WO-31E3	31445	400	-	2.3E-6	8.4E-4
3D-NO-1.4E6	1436919	-	10	2.5E-7	3.3E-5
3D-WO-1.6E6	1637607	12700	-	4.6E-7	4.6E-5

[a]For the size of the smallest and biggest cells, area is shown for 2D meshes and volume for 3D meshes. All values are scaled assuming a radius of 1 for the spherical capsule.

2D cases have been run with both sets of constant properties of Table 2 and with variable properties. 3D cases have been run with the corrected set of constant properties of Table 2 and with variable properties.

3.1 Physical properties

Difficulties have been encountered in the search of the physical properties of n-Octadecane near the melting point. Specially for density of the solid phase and thermal conductivity of both phases, as well as for the fusion temperature. Little information, and sometimes, high disagreements between the different sources has been found.

3.1.1 Constant properties

As a first approximation, physical properties were taken from [2]. The high difference between experimental and numerical results led to the suspicion of being using wrong physical properties. Therefore, a thorough search for physical properties has been carried out. Very little information has been found for some of the properties, as density and thermal conductivity of the solid phase.

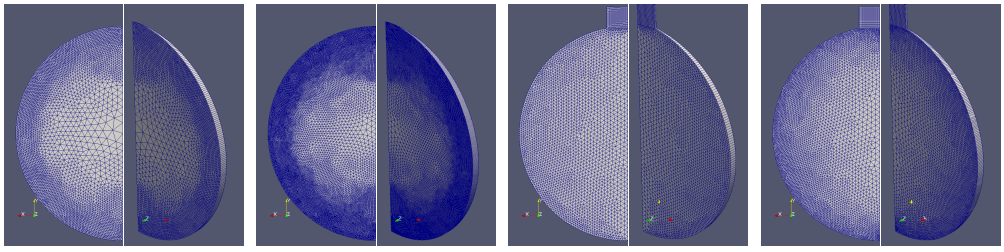

(a) 2D-NO-7.7E3 **(b)** 2D-NO-31E3 **(c)** 2D-WO-5.3E3 **(d)** 2D-WO-9.3E3

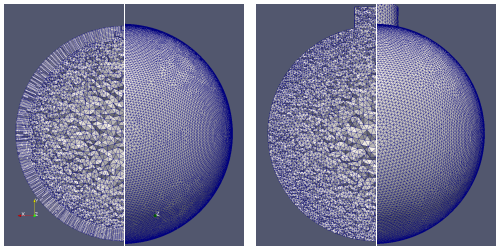

(e) 3D-NO-1.4E6 **(f)** 3D-WO-1.6E6

Figure 1: Meshes used. 2D: Left half of images show a front view, while right half show a tilted view. 3D: Left half of images show a front cut view, while right half show the external surface.

Table 2: Constant physical properties of n-Octadecane

	L (J kg^{-1})	ρ (kg m^{-3})	C_p (J kg^{-1} K^{-1})	λ (W m^{-1} K^{-1})	μ (Pa s)	β (K^{-1})
From [2]	243500	772	2300	0.1505	3.86 E-3	9.1 E-4
Corrected	270159[a]	774.5	2225	0.1505	3.57 E-3	9.46 E-4[b]

[a]Calculated as $242454\frac{\rho_s}{\rho_l}$ in order to have the correct total latent enthalpy, with $\rho_s = 863$ kg/m^3.

[b]Calculated as $\frac{\rho_l(313.15K)-\rho_l(301.33K)}{12.82K}$ from the correlation of liquid density used in the variable properties cases.

3.1.2 Variable properties

- *Melting temperature*: taken from [9]. A fixed value of 301.33 K has been adopted, since several references (e.g. [10]) indicate that n-Octadecane does not present disordered phases between the low temperature oredered solid phase and the liquid phase. There is some disagreement about this value, and values as low as 300.2 K have been reported.Furthermore, it has been seen in the scientific literature (e.g. in [10]) that impurities could modifiy the behaviour of pure n-Octadecane resulting in a modification of the melting temperature, as well as the latent heat of fusion. It is believed, due to the experimental temperature curves presented in [2] that the material used could be melting in a temeperature range around 27-28ºC. This could definitely be a cause of differences between experimental and numerical results.

- *Latent heat of fusion*: 242454 J/kg, from [9]. As mentioned above, this value can

be modified with the presence of impurities.

- *Liquid density*: correlation adopted from [11]. Although the authors of the referred work define a range of validity of their correlation which do not include the temperature range between the melting point and the maximum temperature present in the experiment of Tan et al. [2], comparison with the experimental curve presented in [14] shows a fairly good agreement.

- *Liquid viscosity*: correlation adopted from [12]. This property varies considerably (∼30%) in the temperature range of the experiment.

- *Liquid thermal conductivity*: linearized correlation from [13]. Dispersion of around 5% has been found between data from sources [12, 13], although higher with respect to [15]. In the latter, a value of liquid thermal conductivity of 0.18 W/mK has been reported at the melting point.

- *Liquid specific heat*: linearized correlation from [13].

- *Solid density*: value of 863 kg/m^3 has been adopted. There is high uncertainty in this value, as no exact information has been found. It has been very roughly approximated from the density curve presented in [14].

- *Solid thermal conductivity*: calculated from the value of k_s/k_l presented in [15], with k_l (at the melting temperature) calculated with the correlation of [13]. There is high uncertainty in this value as high dispersion has been found between different sources consulted. The authors believe that the ratio k_s/k_l is the most accurate value of those found in [15] due to its determination procedure, which do not depend on the density of any of the phases.

- *Solid specific heat*: linearized experimental data from [9].

3.2 Initial conditions

Due to the density difference between solid and liquid phases, the upper opening had to be included in the mesh in order to allow the less dense fluid to exit the capsule. Furthermore, an initial condition where a liquid film has already developed near the shell had to be adopted, in order to avoid the formation of liquid cells completely surrounded by solid cells, which would cause divergence due to the impossibility of the less dense fluid to leave the confined cells. The width of this layer is around 3% of the capsule radius (∼1.5 mm), resulting in an initial total liquid fraction of ∼8.5%. Therefore, all numerical simulations in this work are assumed to start in a state corresponding to that of the experiment at t = 12 minutes, which seems to be the time at which liquid fraction is around ∼8.5%.

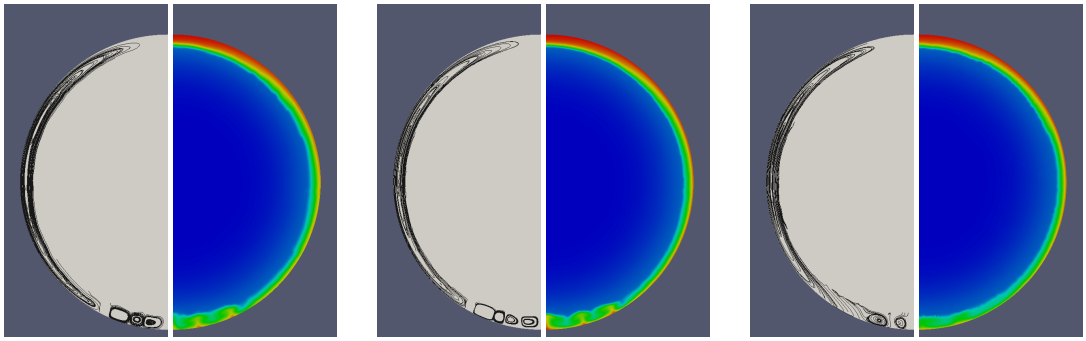

(a) Mesh: 2D-NO-7.7E3 **(b)** Mesh: 2D-NO-31E3 **(c)** Mesh: 3D-NO-1.4E6

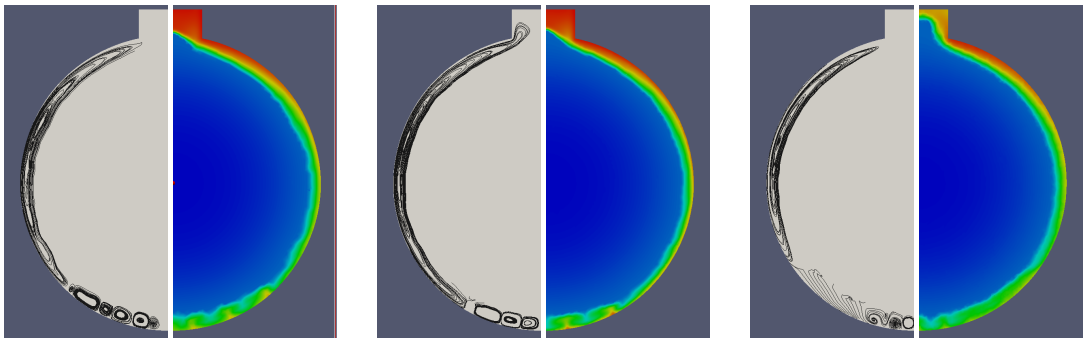

(d) Mesh: 2D-WO-5.3E3 **(e)** Mesh: 2D-WO-9.3E3 **(f)** Mesh: 3D-WO-1.6E6

Figure 2: Vertical cross view of numerical results for 10 min of simulation (t∼22 min in the experiment). Cases with meshes without the upper opening have been run with the corrected constant properties shown in Table 2. Left half of the pictures show streamlines, while right half show temperature maps (blue: cold, red: hot).

4 RESULTS

4.1 Mesh density

Coarse meshes result in faster melting. This pattern is observed for both constant and variable physical properties cases. Cases with variable properties and meshes 2D-WO-31E3 and 3D-WO-1.6E6, are currently running.

Comparing results of cases with constant properties (figs. 2a, 2b, 3a, 3b), it can be observed that 2D results with meshes 2D-NO-7.7E3 and 2D-NO-31E3 are very similar in the sense of the flow patterns encountered. However, there is a better match of the melting rate throughout the whole operation between cases 2D-NO-31E3 (2D) and 3D-NO-1.4E6 (3D).

4.2 2D vs. 3D

There are differences between the flow patterns encountered in 2D and 3D cases. The common feature is the upgoing hot flow close to the shell and downgoing cold flow close

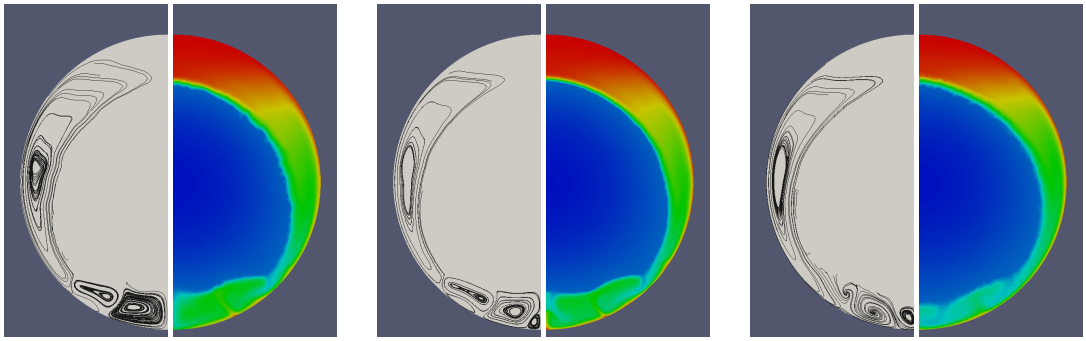

(a) Mesh: 2D-NO-7.7E3 **(b)** Mesh: 2D-NO-31E3 **(c)** Mesh: 3D-NO-1.4E6

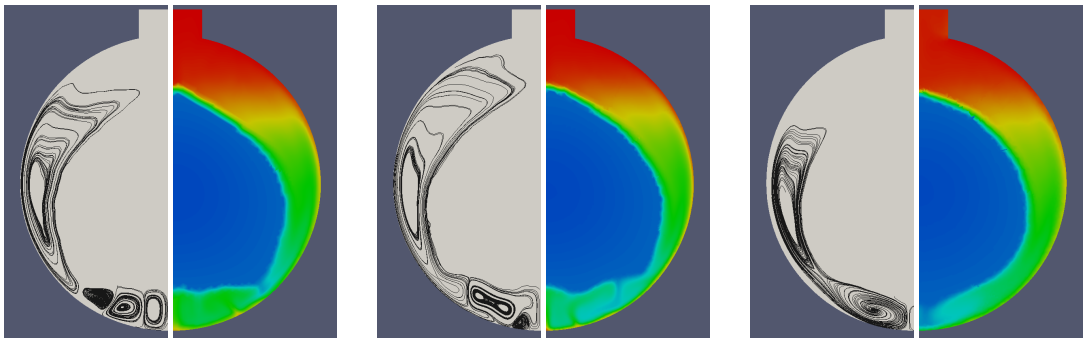

(d) Mesh: 2D-WO-5.3E3 **(e)** Mesh: 2D-WO-9.3E3 **(f)** Mesh: 3D-WO-1.6E6

Figure 3: Vertical cross view of numerical results for 35 min of simulation (t∼47 min in the experiment). Cases with meshes without the upper opening have been run with the corrected constant properties shown in Table 2. Left half of the pictures show streamlines, while right half show temperature maps (blue: cold, red: hot).

to the solid, produced by the gravity force in combination with a decrease of density in the liquid as its temperature increases.

However, in the bottom, due to the unstable thermal layer (hot shell below cold solid), the flow has a highly 3D behaviour. While in 2D cases the fluid eddies formed at the bottom are "trapped"by the fluid eddies of the top/lateral of the capsule (see 2D streamlines in figs. 2 and 3), in 3D cases the high velocity flows generated at the bottom "find their way"to the top of the capsule flowing close to the shell (where the temperature is higher), through some periodically arranged azimuthal angles which alternate with the azimuthal angles where the cold flow comes downwards —close to the solid phase—. Therefore, upward and downward flows show higher and lower velocities in alternate azimuthal angles, as seen in a horizontal cut view (fig. 5). Also, zones of higher and lower temperature of the fluid near the shell are also arranged periodically, in the same way, as seen in figure 4. This effect is high at the bottom and vanishes somewhere below the top of the capsule, where the velocities are lower and a nearly horizontally uniform temperature map is observed in the liquid phase (see figs. 2 and 3).

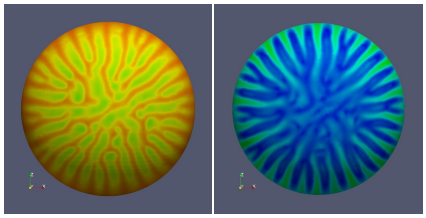

(a) Constant properties; 10 min (t_{exp}∼22 min)

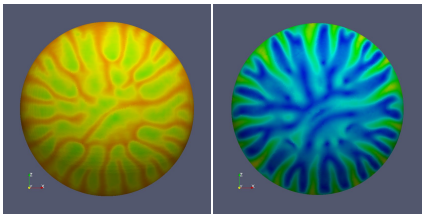

(b) Constant properties; 20 min (t_{exp}∼32 min)

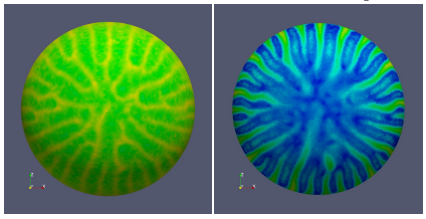

(c) Variable properties; 10 min (t_{exp}∼22 min)

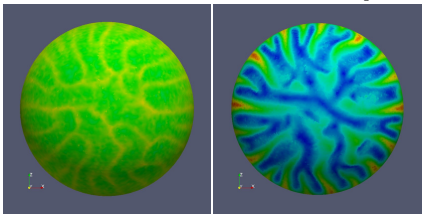

(d) Variable properties; 20 min (t_{exp}∼32 min)

Figure 4: Bottom view of numerical results of 3D cases. In each picture, left half shows a temperature map (red: hot; blue: cold) and right half a velocity magnitude map (red: high; blue: low).

Resulting maximum velocity values of 3D cases are higher than those of 2D cases.

Another effect of this "trapping" of the eddies in 2D cases is that the lower part melts faster than in 3D cases. In the experimental results of Tan et al. [2], the thermometer located at point G ($y = 2.5cm$ above the center) detects that melting there starts before than in point B ($y = 3.75cm$ below the center). In all 2D numerical results reported in this work, point B starts melting before point G, while in 3D cases the opposite happens (see fig. 6). This is taken as an indication of the 3D flow patterns producing a slower melting at the bottom.

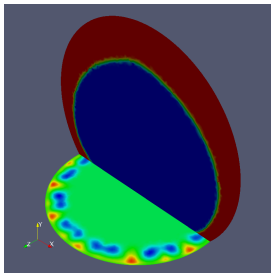

Figure 5: Isometric view of two slice cuts of case 3D-NO-1.4E6 at 35 minutes. Vertical cut shows the different phases (blue: solid; green: interface; red: liquid), while the horizontal cut (at $y = -3cm$) shows a map of vertical velocities (red: highest, upgoing; blue: lowest, downgoing).

4.3 Thermo-physical properties

Regarding the evolution of global melting fraction, cases run with constant properties result in a lower melting rate than those where the variation of properties with temperature

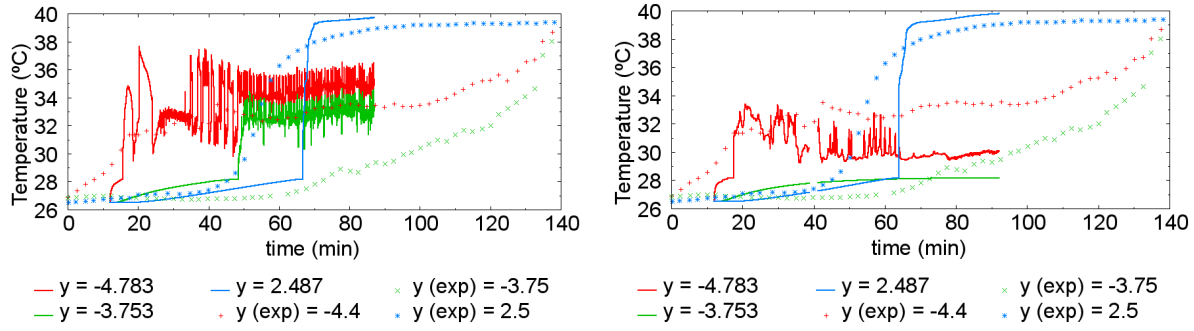

(a) Mesh: 2D-NO-31E3 **(b)** Mesh: 3D-NO-1.4E6

Figure 6: Evolution of T vs. time, for numerical and experimental results (extracted from [2]), at three different locations of the vertical axis (indicated in cm, with $y = 0$ being the center of the capsule).

has been considered. Higher velocities in the liquid are registered in variable properties cases, which is thought to be mainly a result of taking into account the expansion in the melting. Due to these higher velocities, convection is stronger and melting rates higher.

4.4 Differences between experimental and numerical results

As in [2] and [3], numerical results reproduce the qualitative behavior observed in the experiment, but overpredict the velocity at which the melting is produced. As explained in [2], the presence of a base support for holding the sphere in position, could have lowered the heat flow through the bottom of the spherical capsule, extending the melting period as well as weakening the intensity of the unstable thermal layer in this zone.

Furthermore, observing the temperature curves at different positions, it is believed by the authors that the onset of the phase change in the experiment is produced at a lower temperature than the assumed in the simulations (28.18ºC), and may be occurrying in a temperature range, which would explain that the experimental temperature curves stay nearly horizontal around 27ºC and rise more "smoothly"than the numerical results after 28.18ºC.

This smoother rising of the temperature could also be explained partly by the lower temperature and intensity of the unstable thermal layer in the bottom of the capsule.

Comparison of temperature vs. time curves (fig. 6) of numerical and experimental results for various locations indicate that, besides the faster melting, much higher oscillations are shown for the locations below the center of the sphere for the latter. This indicates that velocities higher than those of the experiment may be being predicted in the simulations.

The uncertainty in the value of the solid phase density affects the total amount of latent energy initially contained in the capsule and the velocity of the fluid. The uncertainty in the thermal conductivity of the solid phase affects the velocity in which the solid phase is heated.

5 CONCLUSIONS

Several 2D and 3D numerical simulations of the melting of n-Octadecane inside a spherical capsule have been performed. Cases with constant and variable thermo-physical properties with different meshes have been run and their results analyzed and compared against experimental results from [2]. Modifications in the model and in the numerical treatment with respect to those presented in [3], have been indicated.

In 3D cases, 3D flow patterns are observed at the bottom of the sphere, resulting in periodic arrangements in the azimuthal angle of the upgoing and downgoing flows, with higher maximum velocities of the flow and lower melting rate at the bottom, than in 2D cases. These patterns result in a better match with experimental results.

Regarding the thermo-physical properties used, it is observed that accounting for their variation with temperature results in higher convective fluxes and overall faster melting. It is believed that this effect is mainly due to the expansion in the melting.

Although a better match between experimental and numerical results have been attained with the 3D simulations, the usage of variable thermo-physical properties result in faster melting rates, and therefore in higher differences with the experiment. It is believed that the main cause for these discrepancies are due to not reproducing the thermal boundary conditions accurately, probably overestimating the convection coefficient of the thermal bath and not taking into account its thermal stratification. Furthermore, the significative uncertainties encountered in some properties of n-Octadecane are probably another cause of discrepancies.

ACKNOWLEDGEMENTS

This work has been financially supported by the *Ministerio de Economía y Competitividad, Secretaría de Estado de Investigación, Desarrollo e Innovación*, Spain (ENE-2011-28699), by Termo Fluids S.L., by the Secretaria d'Universitats i Recerca (SUR) del Departament d'Economia i Coneixement (ECO) de la Generalitat de Catalunya and by the European Social Fund.

REFERENCES

[1] Voller, V. and Prakash, C. A Fixed Grid Numerical Modelling Methodology for Convection-Diffusion Mushy Region Phase Change Problems. *Int. J. Heat Mass Tran.* (1987) **30**:1709–1719.

[2] Tan, F.L., Hosseinizadeh, S.F., Khodadadi, J.M., Fan, L. Experimental and computational study of constrained melting of phase change materials (PCM) inside a spherical capsule. *Int. J. Heat Mass Tran.* (2009) **52**:3464–3472.

[3] Galione, P.A., Lehmkuhl, O., Rigola, J., Oliva, A. Fixed-Grid Modeling of Solid-Liquid Phase Change in Unstructured Meshes Using Explicit Time Schemes. *Numer. Heat Transfer B* (2014) **65**:27–52.

[4] Nield, D.A. and Bejan, A. *Convection in Porous Media.* Springer-Verlag, 3d ed., Ch 1 (2006).

[5] Hsu, C.T. and Cheng, P. Thermal Dispersion in a Porous Medium. *Int. J. Heat Mass Tran.* (1990) **33**:1587–1597.

[6] Galione, P.A., Lehmkuhl, O., Rigola, J., Oliva, A., Rodríguez I. Numerical simulations of energy storage with encapsulated phase change materials. Special emphasis on solid-liquid phase change CFD modelling. *Proc. 12th Int. Conf. Energy Storage (INNOSTOCK)* (2012), INNO-SP-56.

[7] Lehmkuhl, O., Pérez-Segarra, C.D., Borrell, R., Soria, M., Oliva, A. TERMOFLUIDS: A new Parallel unstructured CFD code for the simulation of turbulent industrial problems on low cost PC Cluster. *Lect. Notes Comput. Sci. Eng.* (2009) **67**:275–282.

[8] Trias, F.X., Lehmkuhl, O. A Self-Adaptive Strategy for the Time Integration of Navier-Stokes Equations. *Numer. Heat Transfer B* (2011) **60**:116–134.

[9] Messerly, J.F, Guthrie, G.B., Todd, S.S., Finke, H.L. Low-Temperature Thermal Data fpr n-Pentane, n-Heptadecane and n-Octadecane. *J. Chem. Eng. Data* (1967) **12**:338–346.

[10] Broadhurst, M.G. An Analysis of the Solid Phase Behavior of the Normal Paraffins. *J. Res. Natl. Bur. Stand.., A: Phys. Chem.* (1962) **66**:241–249.

[11] Caudwell, D.R., Trusler, J.P.M., Vesovic, V., Wakeham, W.A. The Viscosity and Density of n-Dodecane and n-Octadecane at Pressures up to 200MPa and Temperatures up to 473K. *Int. J. Thermophys.* (2004) **25**:1339–1352.

[12] Yaws, C.L. *Transport Properties of Chemicals and Hydrocarbons.* William Andrew, Ch 3 (2009).

[13] Marano, J.J. and Holder, G.D. A General Equation for Correlating the Thermophysical Properties of n-Paraffins, n-Olefins, and Other Homologous Series. 3. Asymptotic Behavior Correlations for Thermal and Transport Properties. *Ind. Eng. Chem. Res.* (1997) **36**:2399–2408.

[14] Seyer, W.F., Patterson, R.F., Keays, J.L. The Density and Transition Points of the n-Paraffin Hydrocarbons. *J. Am. Chem. Soc.* (1944) **66**:179–182.

[15] Holmen, R., Lamvik, M., Melhus, O. Measurements of the Thermal Conductivities of Solid and Liquid Unbranched Alkanes in the C16-to-C19 Range During Phase Transition. *Int. J. Thermophys.* (2002) **23**:27–39.